optica

Resonant laser spectroscopy of localized excitons in monolayer WSe_2: supplementary material

SANTOSH KUMAR[1,*], MAURO BROTÓNS-GISBERT[2], RIMA AL-KHUZHEYRI[1], ARTUR BRANNY[1], GUILLEM BALLESTEROS-GARCIA[1], JUAN F. SÁNCHEZ-ROYO[1], AND BRIAN D. GERARDOT[1,*]

[1]*Institute of Photonics and Quantum Sciences, SUPA, Heriot-Watt University, Edinburgh EH14 4AS, UK*
[2]*ICMUV, Instituto de Ciencia de Materiales, Universidad de Valencia, P.O. Box 22085, 46071 Valencia, Spain*
[*]*Corresponding author: Santosh.Kumar@hw.ac.uk; B.D.Gerardot@hw.ac.uk*

Published 3 August 2016

This document provides supplementary information to "Resonant laser spectroscopy of localized excitons in monolayer WSe_2," http://dx.doi.org/10.1364/optica.3.000882. Here we summarize the polarization analysis of emitter B and the suppression of fine-structure split lines and binding energy re-normalization under resonant excitation compared to non-resonant excitation. We also present details of the Bayesian approach for estimation of $g^{(2)}(0)$.
http://dx.doi.org/10.1364/optica.3.000882.s001

I. Quantitative analysis of polarization direction

Figure S1(a) shows the color-coded polarization map of emitter B under non-resonant excitation. We fit the spectrum at each polarization rotation angle with sum of 3 Lorentz functions to extract the integrated intensities (closed squares) of all three peaks p_0, p_1 and p_2 that are plotted in Fig. S1(b), (c) and (d), respectively. We fit these intensities with the cosine function (see solid lines) to estimate the polarization directions, which are 97±6, 122±2, and 122±1°for peak p_0, p_1 and p_2, respectively.

II. Suppression of fine-structure split lines

We have investigated the fluorescence spectra of emitter B under four different optical excitation conditions. The blue spectrum in Fig. S2 is for non-resonant excitation at a power of 200 nW and it shows three fine-structure-split peaks p_0, p_1 and p_2 and almost no emission from the BS-X state ≈+4.75 meV away from p_1. The peak intensity ratio between p_1 and p_2 (I_{p1}/I_{p2}) under non-resonant excitation is ≈ 2. Figure S2 also shows fluorescence spectra under resonant excitation to the BS-X state (magenta), p_1 (black), and p_0 (red). The brightest peaks for magenta and red spectra are the scattered laser, which has been subtracted for the black spectrum. These spectra show that the emission intensity of p_2 under resonant excitation conditions is suppressed by an order of magnitude. This observation gives hints that a specific valley-index is optically addressed with quasi- or true resonant excitation. Further evidence is provided by Fig. S3, which shows the I_{p1}/I_{p2} ratio, shown by closed circles, increases as we go from near-resonance excitation to true resonance excitation of p_2. The blue-band is for I_{p1}/I_{p2} ratio with standard deviation measured by non-resonant PL.

III. Binding energy re-normalization

We use the high-resolution PLE technique, as discussed in the main text, to investigate the effect of (quasi-) resonant excitation on the binding energy of the two fine-structure split peaks p_1 and p_2 from emitter B. The time traces of p_1 and p_2 under resonant excitation of peak p_0 and non-resonant excitation are shown in Fig S4a and S4b, respectively. Figures S4c and S4d show histograms of binding energies E_B^{12} (= E_{p2} - E_{p1}) extracted by fitting the spectra of Fig. S4a and S4b, respectively. The statistical distribution of E_B^{12} under resonant (non-resonant) excitation is centered at 280 ± 10 (340 ± 10) μeV, and therefore yields a 60 μeV binding energy re-normalization of E_B^{12}. The spectral jitter is similar in each case. We also investigated binding energies E_B^{01} (= E_{p1} - E_{p0}) under excitation wavelengths 784.3800 and 784.4090 nm, as shown in Fig. 3c. Here we observe E_B^{01} = ∼600 μeV, identical to non-resonant excitation energy separation. We do not currently understand the details of the binding energy re-normalization or the origin and nature of the different peaks.

IV. Bayesian approach for $g^{(2)}(0)$ estimation

Under CW excitation the 2nd order autocorrelation of the emitted photons is given by

$$f(\tau) = I_0 g^{(2)}(\tau) = I_0(1 - \rho^2 \exp(-|\tau|/\tau_1), \qquad \textbf{(S1)}$$

where, $\tau = t - t_0$ is the time delay between coincidences, t_0 is electrical the time delay between two APD channels, τ_1 is the decay-time of the emission signal, which under zero power limit gives the lifetime of the signal, and the signal-to-background ratio is

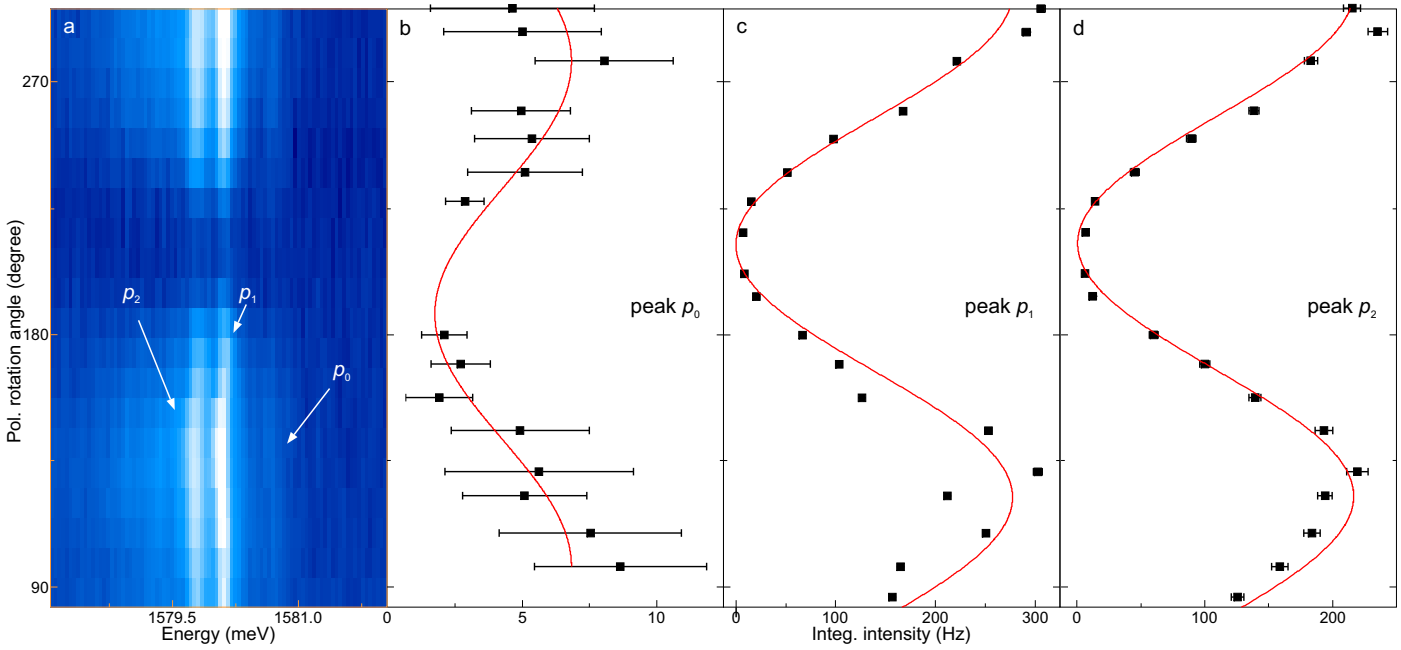

Fig. S1. (a) Color-coded polarization map of emitter B under non-resonant excitation at $\lambda = 532$ nm and at a power of 1 µW. Integrated intensities of peaks (b) p_0, (c) p_1, and (d) p_2 as a function of polarization rotation angle as extracted from (a). The solid lines are cosine fits.

given by $\rho/(1-\rho)$. The system response function is given by,

$$g(\tau) = \exp\left(-\log(4)\frac{\tau^2}{\gamma^2}\right), \qquad \textbf{(S2)}$$

where, an instrument response time $\gamma = 0.75$ ns (combined for both detectors and the timing electronics) was measured and is used for analysis of all antibunching data presented in this letter. The experimental data is modelled using the convolution of the 2$^{\text{nd}}$ order correlation function (see Eq. S1) and the instrument response function (Eq. S2) using a Bayesian approach[1, 2]. The convolved equation is given by:

$$M(t_i; I_0, \rho, \tau_1, t_0, \gamma) = (f * g)(t) \qquad \textbf{(S3)}$$

First, we constructed the posterior probability distribution for the model parameters,

$$P(I_0, \rho, \tau_1, t_0 | D, \gamma) \propto P(D | I_0, \rho, \tau_1, t_0, \gamma) P(I_0, \rho, \tau_1, t_0), \qquad \textbf{(S4)}$$

where the first term on the right hand side represents the likelihood of the data given a set of parameters and the second term the prior distribution of the parameters which we assume here to uniform multidimensional probability distribution with appropriate bounds. Under certain assumptions and subject to Gaussian noise the likelihood is given by:

$$P(D | I_0, \rho, \tau_1, t_0, \gamma) = \exp\left(-\sum_i \frac{(y_i - M(t_i; I_0, \rho, \tau_1, t_0, \gamma))^2}{2\sigma_i^2}\right), \qquad \textbf{(S5)}$$

the sum is carried over all experimental data points $\{t_i, y_i, \sigma_i\}$, where, y_i is the coincidences counts measured at time t_i and σ_i is the square-root noise assumption for y_i. The prior probabilities for the model parameters were taken to be uniform distributions with appropriate bounds.

The most probable parameters are obtained from the optimization of the posterior distribution, which in our case is equivalent to a least-square fit. In order to study the full posterior distribution we sample it using the Metropolis-Hastings algorithm[3]. From the obtained samples we can approximate the marginal distributions of all four parameters of the convolved function (see Fig. S5 for emitter C).

We obtain the probability density function of normalized 2$^{\text{nd}}$ order correlation function at zero time, $g^{(2)}(\tau = 0) = 1 - \rho^2$ using the distribution of ρ. The use of Bayesian methods allows us to give appropriate error bounds even when the parameter distribution is highly non-Gaussian as is the case for the background parameter ρ in Fig. S5.

REFERENCES

1. D. S. Sivia, *Data analysis: a Bayesian tutorial* (Oxford university press, 1996).
2. J. L. Puga, M. Krzywinski, and N. Altman, "Points of significance: Bayesian statistics," Nat. Methods **12**, 377 (2015).
3. N. Metropolis, A. W. Rosenbluth, M. N. Rosenbluth, A. H. Teller, and E. Teller, "Equation of state calculations by fast computing machines," J.Chem. Phys. **21**, 1087 (1953).

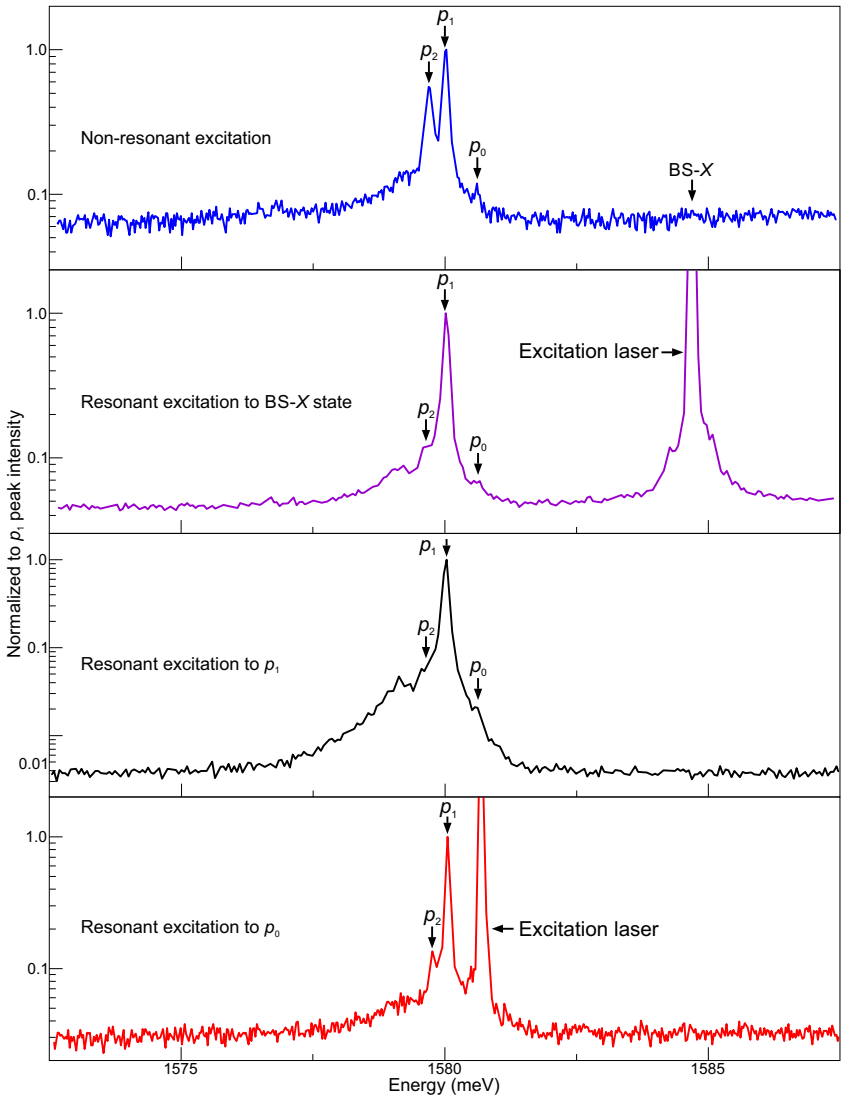

Fig. S2. The fluorescence spectra of emitter B under non-resonant excitation (blue) and under resonant excitation to the BS-X (magenta), peak p_1 (black), and peak p_0 (red). Emission of peak p_2 is highly suppressed under resonant excitation conditions.

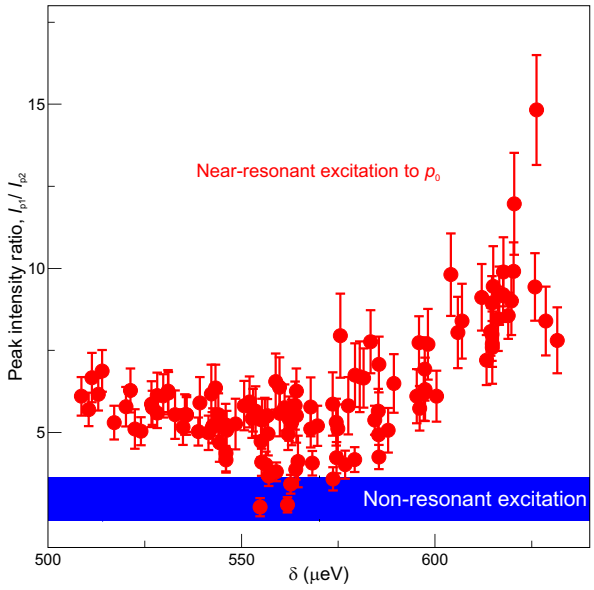

Fig. S3. Detuning-dependent peak intensity ratio of the peak p_1 to the peak p_2 (I_{p1} / I_{p2}) under near-resonant excitation to the p_0 resonance (closed circles) extracted from the time-trace shown in Fig. S4a. The blue-band represents the I_{p1} / I_{p2} ratio with standard deviation under non-resonant excitation extracted from the time-trace shown in Fig. S4b.

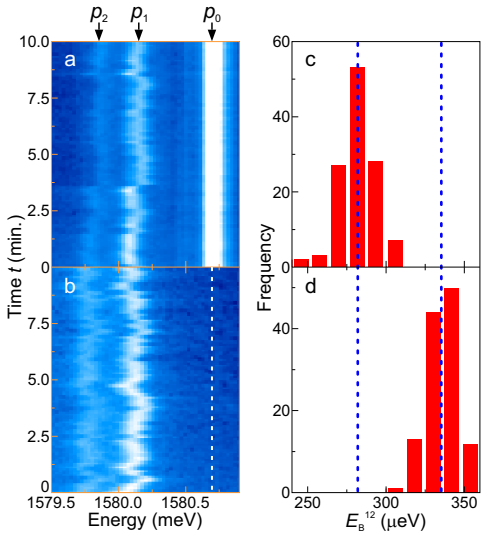

Fig. S4. Time traces of high-resolution fluorescence spectra of emitter B under **a,** resonant excitation of line p_0 at $\lambda = 784.3666$ nm at a power of 4 μW and **b,** non-resonant excitation at a power of 11 μW. **c, d,** Histograms of the binding energy (E_B^{12}) extracted from time traces in (a,b).

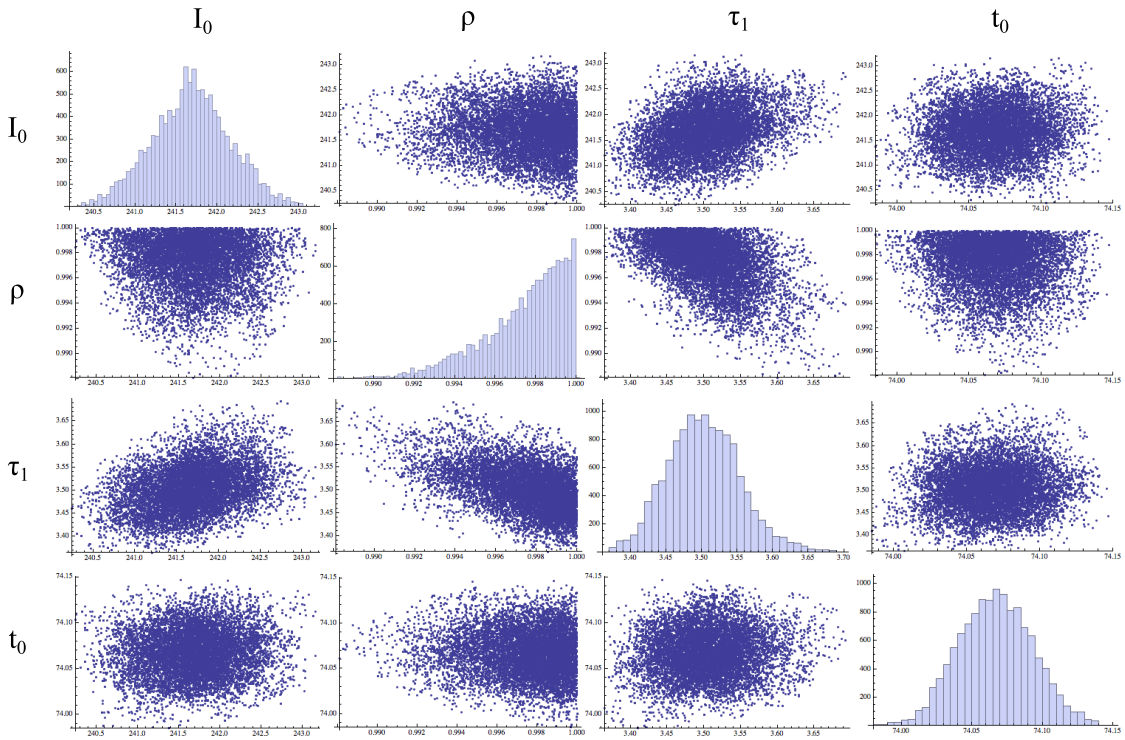

Fig. S5. Samples obtained from the posterior distribution of all four parameters used for fitting the antibunching data of emitter C shown in Fig.4d of the main text. The Metropolis-Hastings algorithm was used for obtaining the samples. The diagonal plots show an approximation to the marginal distribution of the model parameters obtained from the samples and the off-diagonal plots show the samples projected onto the subspace of two parameters.